Mechanism of transport of IFT particles in *C. elegans* cilia by the concerted action of kinesin-II and OSM-3 motors

Xiaoyu Pan,[1] Guangshuo Ou,[1] Gul Civelekoglu-Scholey,[1] Oliver E. Blacque,[2] Nicholas F. Endres,[3,4] Li Tao,[1] Alex Mogilner,[1] Michel R. Leroux,[2] Ronald D. Vale,[3,4] and Jonathan M. Scholey[1]

[1]Section of Molecular and Cellular Biology, Center for Genetics and Development, University of California, Davis, Davis, CA 95616
[2]Department of Molecular Biology and Biochemistry, Simon Fraser University, Burnaby, British Columbia V5A 1S6, Canada
[3]Howard Hughes Medical Institute and [4]Department of Cellular and Molecular Pharmacology, University of California, San Francisco, San Francisco, CA 94107

THE JOURNAL OF CELL BIOLOGY

The assembly and function of cilia on *Caenorhabditis elegans* neurons depends on the action of two kinesin-2 motors, heterotrimeric kinesin-II and homodimeric OSM-3–kinesin, which cooperate to move the same intraflagellar transport (IFT) particles along microtubule (MT) doublets. Using competitive in vitro MT gliding assays, we show that purified kinesin-II and OSM-3 cooperate to generate movement similar to that seen along the cilium in the absence of any additional regulatory factors. Quantitative modeling suggests that this could reflect an alternating action mechanism, in which the motors take turns to move along MTs, or a mechanical competition, in which the motors function in a concerted fashion to move along MTs with the slow motor exerting drag on the fast motor and vice versa. In vivo transport assays performed in Bardet-Biedl syndrome (BBS) protein and IFT motor mutants favor a mechanical competition model for motor coordination in which the IFT motors exert a BBS protein–dependent tension on IFT particles, which controls the IFT pathway that builds the cilium foundation.

Introduction

Cilia are microtubule (MT)-based nanomachines that perform diverse roles in motility, sensory perception, and signaling, and their dysfunction contributes to ciliary diseases (Rosenbaum and Witman, 2002; Scholey, 2003; Pan et al., 2005; Badano et al., 2006; Scholey and Anderson, 2006). Cilia are built and maintained by intraflagellar transport (IFT) motors that deliver ciliary precursors bound to protein complexes called IFT particles (consisting of subcomplexes IFT-A and -B; Cole et al., 1998) from the basal bodies to their sites of incorporation into cilia (Scholey, 2003). Understanding the mechanism of IFT and how defects in this process contribute to ciliary diseases is currently a topic of great interest.

One ciliopathy that may reflect defects in IFT is Bardet-Biedl syndrome (BBS), a genetically heterogeneous disorder characterized by a pleiotropic phenotype that encompasses truncal obesity, pigmentary retinopathy, polydactyly, renal malformations, learning disabilities, hypogenitalism, and anomisa

(Beales, 2005). Mutations in 11 BBS genes are thought to cause defects in basal bodies or cilia, which may be a significant factor underlying this disease (Ansley et al., 2003; Blacque et al., 2004; Badano et al., 2006). In *Caenorhabditis elegans*, BBS proteins control the IFT motors that build cilia on sensory neurons, and, consequently, *C. elegans* sensory cilia represent an appealing model to address mechanisms of IFT and the roles of BBS proteins in cilium biogenesis and disease (Ou et al., 2005).

C. elegans amphid channel ciliary axonemes are made up of two domains: an initial segment (called the middle segment) containing 4-μm–long MT doublets extending from the 1-μm–long transition zone (a modified basal body that is also called the proximal segment) that together form the cilium foundation and a distal segment comprising 2.5-μm–long MT singlets (Perkins et al., 1986). We have previously shown that the IFT particles assembling these sensory cilia are moved by the coordinate action of two anterograde IFT motors called kinesin-II and OSM-3, which are both members of the kinesin-2 family (Cole et al., 1993; Shakir et al., 1993; Lawrence et al., 2004; Snow et al., 2004). These motors function redundantly to move the same IFT particles along the initial segment and build the cilium foundation, with either motor but not both being dispensable for

X. Pan and G. Ou contributed equally to this paper.

Correspondence to Jonathan M. Scholey: jmscholey@ucdavis.edu

Abbreviations used in this paper: BBS, Bardet-Biedl syndrome; IFT, intraflagellar transport; MT, microtubule.

The online version of this article contains supplemental material.

this function (Snow et al., 2004; Evans et al., 2006). Then, OSM-3 alone extends singlet MTs on the distal ends of the cilium core in a process involving OSM-3 movement along these distal singlets (Perkins et al., 1986; Snow et al., 2004; Evans et al., 2006).

In this study, we focus on the question of how kinesin-II and OSM-3 are functionally coordinated to move the same IFT particle along the initial segment of amphid channel cilia. The rates of IFT seen in *osm-3, klp-11*, and *kap-1* mutants suggest that kinesin-II alone moves along MTs at 0.5 µm/s and OSM-3 alone moves at 1.3 µm/s. This also suggests that the intermediate rate of transport seen in the initial segment of wild-type cilia (0.7 µm/s) results from the action of both motors (Snow et al., 2004; Ou et al., 2005), but the rates of MT motility predicted for the purified motors have not been tested using in vitro motility assays.

A related question is how BBS proteins contribute to the functional coordination of kinesin-2 motors. In *C. elegans*, BBS-1, -2, -3, -5, -7, and -8 were shown to be ciliary proteins (Blacque et al., 2004), and, of these, the loss of BBS-7 and -8 function in mutant animals leads to the loss of ciliary distal segments and sensory defects (Blacque et al., 2004). Using in vivo transport assays, we observed that in wild-type animals, IFT

particle subcomplexes IFT-A and -B move together along the initial segment with kinesin-II and OSM-3 at a single rate of 0.7 µm/s. However, in *bbs*-7/-8 mutants, kinesin-II and IFT-A move together at 0.5 µm/s, but OSM-3–kinesin and IFT-B move as a distinct complex at 1.3 µm/s. This suggested that BBS-7/-8 proteins coordinate IFT by holding subcomplexes IFT-A and -B together and stabilizing the integrity of the IFT particles (Ou et al., 2005). This offers a unique system for probing the mechanism by which BBS proteins contribute to kinesin-II and OSM-3 motor coordination.

The power of *C. elegans* as a system for addressing these questions would be enhanced if in vivo time-lapse microscopy assays of IFT (Orozco et al., 1999) could be complemented by in vitro motility assays (Vale et al., 1985), but this has not been performed because of the low abundance of native kinesin-2 motors (Signor et al., 1999). Here, we have initiated such in vitro assays using purified recombinant *C. elegans* kinesin-II and OSM-3.

In this study, we combine both in vivo and in vitro motility assays of kinesin-II and OSM-3 to determine (1) whether the cooperative motility observed in cilia is an intrinsic property of the motors alone or whether it depends on additional ciliary factors; (2) what the mechanism is by which the two IFT kinesins
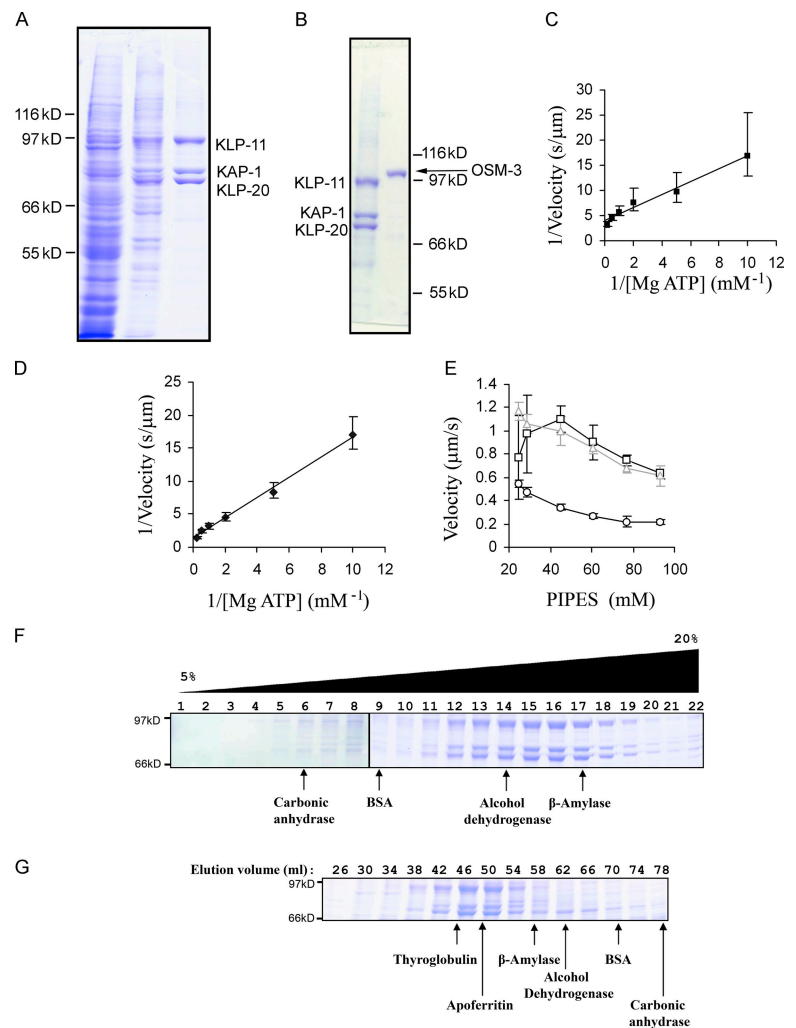

Figure 1. **Preparation and characterization of recombinant *C. elegans* kinesin-II and OSM-3.** (A) SDS gels of Sf9 cell high speed supernatant (left), Talon column eluate (middle), and Sephacryl S-300 purified kinesin-II (right). (B) SDS gels of purified kinesin-II and OSM-3. (C and D) Double reciprocal plots of kinesin-II– (C) and OSM-3 (D)–driven MT motility versus [Mg-ATP] in standard MT gliding assays. (E) MT gliding velocity driven by kinesin-II (circles), OSM-3 (squares), and OSM-3–G444E (triangles) under standard assay conditions but varying concentrations of K$_2$-Pipes. Error bars represent the standard deviations. (F and G) On sucrose density gradients (F) and gel filtration columns (G), the KLP-11, KAP-1, and KLP-20 subunits elute as a monodisperse heterotrimeric complex (S value = 9.8; Rs = 7.1 nm; and native molecular mass = 287 kD) in a KLP-11/KLP-20/KAP-1 molar stoichiometry of 1.0:1.17:0.89 (protein standard peak positions are also indicated).

cooperate to move IFT particles to redundantly assemble the cilium foundation and whether motor cooperation contributes to the dissociation of the IFT particles in the *bbs* mutants; and (3) whether we can develop quantitative models for motor coordination that account for the in vivo and in vitro velocities of the motors. The results illuminate the mechanism by which the two same-polarity IFT motors cooperate to move an IFT particle along a cilium.

Results

Motility of purified kinesin-II and OSM-3

The question of whether the motor coordination that gives rise to an intermediate rate of transport is an intrinsic property of the motors or whether it requires additional ciliary cofactors can be addressed using competitive in vitro motility assays with mixtures of purified kinesin-II and OSM-3. Because it is difficult to purify native holoenzymes of kinesin-II and OSM-3 from *C. elegans* (Signor et al., 1999), we used baculovirus and *Escherichia coli* systems to overexpress and purify recombinant kinesin-II (see next paragraph) and OSM-3 (Fig. 1, A and B; see Imanishi et al. on p. 931 of this issue), and we sought conditions under which these preparations drive motility at the rates predicted from in vivo experiments (Snow et al., 2004).

Purified kinesin-II behaved as a monodisperse, heterotrimeric complex on sucrose gradients (Fig. 1 F) and gel filtration columns (Fig. 1 G) consisting of 1 mol each of its subunits KLP-11, KLP-20, and KAP-1 with a native molecular mass of 287 kD (supplemental material and Fig. S1, available at http://www.jcb.org/cgi/content/full/jcb.200606003/DC1). These hydrodynamic properties are very similar to those of the native kinesin-II holoenzyme in *C. elegans* extracts (Signor et al., 1999). In MT gliding assays, kinesin-II–driven motility conformed to Michaelis-Menten kinetics with a nucleotide profile very similar to that of kinesin-1 (Cohn et al., 1989), indicating that Mg-ATP is the preferred substrate for kinesin-2 motors (Table I, supplemental material, and Fig. S2).

In MT gliding assays performed under standard conditions (in BRB80, which contains 80 mM Pipes), we observed that purified kinesin-II and OSM-3 both used Mg-ATP according to Michaelis-Menten kinetics (Fig. 1, C and D). However, kinesin-II

alone moved MTs at a maximal rate of 0.3 μm/s, and OSM-3 alone moved them at 0.7 μm/s. Although the relative rates of motility driven by the two motors were consistent with in vivo transport assays, the actual rates observed in vitro were approximately twofold lower than those seen in vivo. Therefore, we sought in vitro assay conditions that supported the rates of transport observed in vivo and found that by lowering the K_2-Pipes buffer concentration, rates very similar to those predicted from in vivo assays were observed (Fig. 1 E; also see next section).

Recombinant OSM-3 is purified in an active homodimeric state, but it displays autoinhibition and drives a low MT gliding velocity (0.3 μm/s) when assayed on antibody-coated surfaces, and it can be activated by the mutagenesis of glycine residue 444 to glutamate (Snow et al., 2004; Imanishi et al., 2006). To control for this potential complication, we compared MT gliding driven by wild-type OSM-3 on antibody-coated surfaces or directly coated onto the coverslip with that of the OSM-3–G444E mutant protein in different Pipes concentrations (Fig. 1 E) and observed that directly adsorbed OSM-3 and OSM-3–G444E both supported MT gliding at similar rates of 1.1 and 0.97 μm/s, respectively. We conclude that direct adsorption onto the coverslip, as in our standard gliding assays, activates autoinhibited OSM-3 to the same extent as mutagenesis, and, consequently, the assays of both the wild-type OSM-3 and OSM-3–G444E discussed in the following section refer to the active state.

Purified kinesin-II and OSM-3–kinesin interact to produce intermediate rates of motility in MT gliding assays

Based on the aforementioned results, we analyzed the rate of MT-based motility driven by mixtures of varying molar ratios of pure kinesin-II and OSM-3 in the presence of 45 mM Pipes for wild-type OSM-3 and 25 mM Pipes for OSM-3–G444E (Fig. 2 and Table II). Under these optimized conditions, kinesin-II alone moved at ∼0.5 μm/s, whereas OSM-3 alone (wild type or the G444E mutant) moved at ∼1.1 μm/s (Fig. 1 E, Fig. 2, Table II, and Video 1; available at http://www.jcb.org/cgi/content/full/jcb.200606003/DC1), which is very close to the rates of transport driven by kinesin-II (0.5 μm/s) and OSM-3 (1.3 μm/s) in vivo (Snow et al., 2004; Ou et al., 2005). Moreover, mixtures of the two motors displayed intermediate rates of motility, with the

Table I. **Summary of the kinetic parameters of recombinant *C. elegans* kinesin-II and sea urchin kinesin-1**

Substrate or inhibitor	Recombinant *C. elegans* kinesin-II	Sea urchin kinesin-1
Mg-ATP	K_m = 0.28 ± 0.05 mM V_{max} = 0.26 ± 0.01 μm/s	K_m = 0.063 ± 0.034 mM V_{max} = 0.56 ± 0.10 μm/s
Mg-GTP	K_m = 5.5 mM V_{max} = 0.058 μm/s	K_m = 1.9 ± 0.8 mM V_{max} = 0.43 ± 0.08 μm/s
Mg-ADP	Competitive inhibitor K_i = 0.042 mM	Competitive inhibitor K_i = 0.156 ± 0.052 mM
Mg-ATP–γ-S[a]	Competitive inhibitor K_i = 0.31 mM	Competitive inhibitor K_i = 0.014 ± 0.003 mM
Pi	Competitive inhibitor K_i = 4.4 mM	Unknown
Mg-AMPPCP	Inhibitor - not a competitive inhibitor	Inhibitor - not a competitive inhibitor
Mg-AMPPNP	Inhibitor - not a competitive inhibitor	Inhibitor - not a competitive inhibitor

[a]Mg-ATP–γ-S can be used as an alternative substrate by recombinant *C. elegans* kinesin-II. The velocity is 0.0100 ± 0.0015 μm/s at 2 mM Mg-ATP–γ-S.
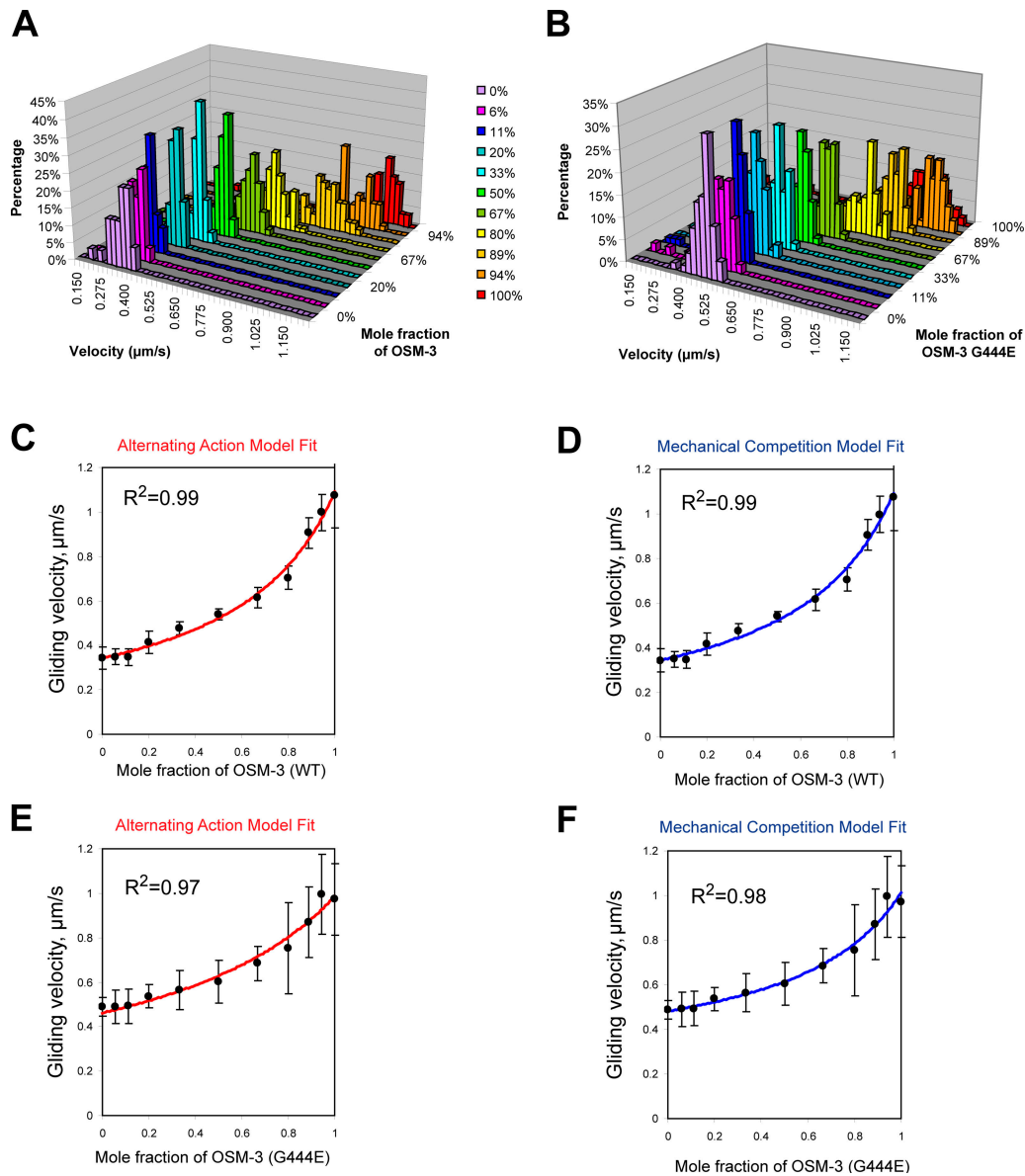
Figure 2. **MT gliding rate versus mole fraction for mixtures of OSM-3 and kinesin-II showing alternating action and mechanical competition model fits.** (A and B) Velocity histograms of gliding rates in competitive motility assays as a function of the percentage of wild-type OSM-3 (A) and OSM-3–G444E mutant (B) versus kinesin-II. Between 0 and 100% OSM-3, gliding rates intermediate between those produced by each motor alone are observed. (C and D) Gliding assay plotted versus mole fraction of wild-type (WT) OSM-3. Experimental data (black dots) with standard deviations (error bars) are shown with best fits for the alternating action (red line; C) and the mechanical competition (blue line; D) models. The parameters are as follows: $v_{kinesin-II} = 0.34$ μm/s and $v_{osm-3} = 1.09$ μm/s (C); and $V_{kinesin-II}^{max} = 0.34$ μm/s, $V_{osm-3}^{max} = 1.09$ μm/s, and $\gamma = 0.98 \approx 1$ (D). (E and F) Gliding assay velocities plotted versus mole fraction of OSM-3–G444E. Experimental data (black dots) with standard deviations are shown with the best fit for the alternating action (red line; E) and the mechanical competition (blue line; F) models. The parameters are as follows: $v_{kinesin-II} = 0.46$ μm/s and $v_{osm-3} = 0.99$ μm/s (E); and $V_{kinesin-II}^{max} = 0.48$ μm/s, $V_{osm-3}^{max} = 1$ μm/s, and $\gamma = 0.7$ (F).

rate varying in a nonlinear fashion with the molar ratio and replicating the in vivo rate of 0.7 μm/s at a mole fraction of OSM-3 between 0.6 and 0.8 (Fig. 2, Table II, and Video 1). This suggests that intermediate velocities of motility, like those observed along the initial segments of cilia, can be generated by simple functional interactions between kinesin-II and OSM-3 without any requirement for additional ciliary factors such as regulators of motility, the presence of IFT particles bound to the motors as cargo, an overlying ciliary membrane, or cilia-specific axonemal MT doublets to serve as tracks for the motors.

Models for the functional coordination of the two anterograde IFT kinesins

The observation that kinesin-II and OSM-3 cooperate to drive MT motility at an intermediate rate that depends on their molar ratio can be explained using two types of models, as described in detail in the supplemental material. In the first model, the alternating action model, we propose that the motors act sequentially so that a fast step or a run of several fast steps driven by OSM-3 alternates with a slow step or a run of slow steps taken by kinesin-II (Fig. S3 A, available at

Table II. **MT gliding velocities in the competitive motility assays with wild-type OSM-3 and OSM-3–G444E mutant versus kinesin-II**

Parameter	Value for each assay										
Kinesin-II and OSM-3											
Kinesin-II (μM)	0.00	0.29	0.56	1.00	1.67	2.50	3.33	4.00	4.44	4.71	5.00
OSM-3 (μM)	5.00	4.71	4.44	4.00	3.33	2.50	1.67	1.00	0.56	0.29	0.00
Mole fraction of OSM-3 (%)	100	94	89	80	67	50	33	20	11	6	0
Mean velocity (μm/s)	1.075	0.998	0.906	0.705	0.615	0.540	0.476	0.415	0.347	0.348	0.343
Standard deviation (μm/s)	0.148	0.083	0.069	0.052	0.047	0.025	0.030	0.051	0.039	0.036	0.052
Count of MTs	55	63	57	74	59	74	63	58	53	49	30
Kinesin-II and OSM-3–G444E											
Kinesin-II (μM)	0.00	0.29	0.56	1.00	1.67	2.50	3.33	4.00	4.44	4.71	5.00
OSM-3–G444E (μM)	5.00	4.71	4.44	4.00	3.33	2.50	1.67	1.00	0.56	0.29	0.00
Mole fraction of OSM-3–G444E (%)	100	94	89	80	67	50	33	20	11	6	0
Mean velocity (μm/s)	0.973	0.995	0.869	0.754	0.684	0.603	0.564	0.537	0.493	0.490	0.488
Standard deviation (μm/s)	0.162	0.180	0.159	0.204	0.077	0.096	0.086	0.052	0.078	0.076	0.043
Count of MTs	55	66	66	68	73	71	61	66	71	50	67

http://www.jcb.org/cgi/content/full/jcb.200606003/DC1). The periodic switching of the two motors would average out to produce the intermediate velocity of motility observed in vitro and along the cilium. In the second model, the mechanical competition model, the motors act simultaneously in a concerted fashion, with the slower moving kinesin-II exerting drag on the faster OSM-3 and the faster moving OSM-3 pulling kinesin-II along and speeding it up (Fig. S3 B). We developed quantitative alternating action and mechanical competition models from which we derived equations that relate the speed of motility to the mole fraction of the two motors (supplemental material). We observed that by using reasonable parameter adjustments, the equations derived from both models displayed excellent fit to the data points in plots of MT gliding velocity versus the mole fraction of OSM-3 (Fig. 2, C–F), and, thus, the two models can account for the gliding assay data and the rates of IFT particle transport observed along the cilia of wild-type, *klp-11*, and *osm-3* animals (see Discussion). Thus, a significant conclusion from our quantitative modeling is that both the alternating action and the mechanical competition models are highly plausible, but this analysis by itself did not allow us to decide whether alternating action or mechanical competition is the more likely mechanism of motor coordination.

However, the alternating action and mechanical competition models do make distinct predictions concerning the transport of IFT particles in double mutants lacking BBS proteins and either kinesin-II or OSM-3 (*bbs;klp-11*, *bbs;kap-1*, or *bbs;osm-3* mutants). Let us consider why IFT particle subcomplexes A and B apparently move together along the initial segment of the cilium at 0.7 μm/s in wild types, whereas in *bbs* mutants, IFT-A is apparently moved by kinesin-II at 0.5 μm/s, and IFT-B is moved at ∼1.1–1.3 μm/s by OSM-3 (Ou et al., 2005). We assume that the BBS proteins stabilize intact IFT particles, which therefore dissociate into IFT-A and -B in the *bbs* loss of function mutants. Although this dissociation could be passive, we reasoned that it might instead be an active process caused by stresses imposed on the IFT particles by the concerted action of kinesin-II and OSM-3 motors moving the IFT particles together if the slow motor exerts drag on the fast motor and vice versa, as in the mechanical competition model (supplemental material).

Such stresses could not be developed by motors acting sequentially, as in the alternating action model, because only one type of motor will be moving the particle at any one time (supplemental material). Furthermore, if the stresses that dissociate IFT particles in *bbs* single mutants require mechanical competition between kinesin-II and OSM-3, the loss of either motor together with BBS protein function, as in *bbs;kinesin-2* double mutants, should prevent IFT particle dissociation. Based on these arguments, the alternating action model predicts that in double *bbs;kinesin-2* mutants, IFT particles will dissociate passively into IFT-A and -B, only one of which is moved along the cilium (Fig. 3 A). On the other hand, the mechanical competition model predicts that the IFT particles should remain intact in the absence of the tension exerted on IFT particles by the concerted action of the competing motors (Fig. 3 A).
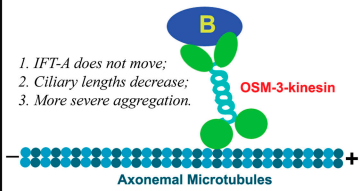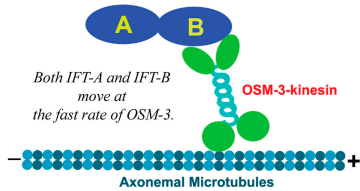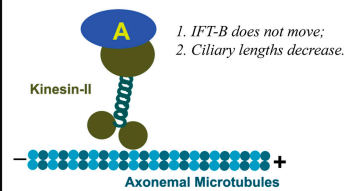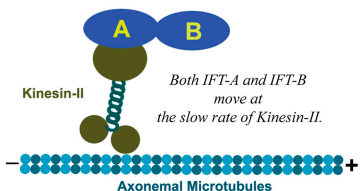
Testing the models by in vivo transport assays in *bbs;kinesin-2* double mutants

We tested the aforementioned model predictions by assaying IFT and examining the ciliary phenotypes in *bbs-7/-8;klp-11* and *bbs-7/-8;osm-3* double mutants. Specifically, we made double mutant strains using CHE-11::GFP to mark IFT-A and CHE-2::GFP or OSM-6::GFP to track IFT-B. In wild-type animals, as we demonstrated before, CHE-11::GFP and CHE-2::GFP move identically along both initial and distal segments of sensory cilia (Fig. 4, A and C), but in *bbs-7* single mutants (Fig. 4, B and D), IFT particles A and B dissociate and move separately (Ou et al., 2005). Significantly, however, in *bbs-7/-8; klp-11* double mutants (Fig. 4, E, F, I, J, and M; Table III, and Videos 2 and 4; available at http://www.jcb.org/cgi/content/full/jcb.200606003/DC1), CHE-11::GFP enters the distal segments and moves at the same velocity as CHE-2::GFP or OSM-6::GFP, which is characteristic of OSM-3–kinesin's fast speed along both the initial and distal segments. In *bbs-7/-8;osm-3* double mutants (Fig. 4, G, H, K, L, and N; Table III, and Videos 3 and 5), both CHE-2::GFP and OSM-6::GFP enter the remaining initial segments and are moved by kinesin-II at its characteristic slow velocity.
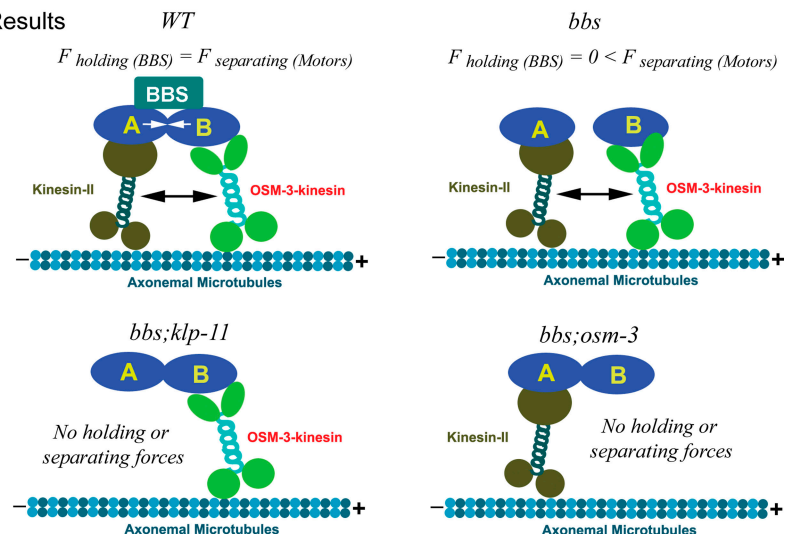
Thus, we observed the following: (1) The *bbs-7/-8;klp-11* and *bbs-7/-8;osm-3* double mutants have phenotypes identical

Figure 3. Model showing BBS proteins antagonizing mechanical competition between kinesin-II and OSM-3 to maintain IFT particle integrity. (A) Demonstrates distinct phenotypes predicted by the two models in *bbs-;motor* double mutants. The alternating action model predicts that in *bbs-;klp-11* double mutants, IFT-A cannot be moved by either kinesin-II or OSM-3–kinesin and will not enter cilia, so IFT-A will form aggregates in the endings of truncated cilia, mimicking the phenotype of IFT-A mutants. On the other hand, in *bbs-;osm-3* double mutants, IFT-B cannot be moved by kinesin-II or OSM-3, and ciliary length will decrease. In contrast, the mechanical competition model predicts that in either *bbs-;klp-11* or *bbs-;osm-3* double mutants, there will be no mechanical competition between the two motors or no drag exerted through IFT particles, so even in the absence of BBS proteins, IFT particles can be maintained in a single complex, and A and B subcomplexes will display identical transport profiles. (B) Summary of the results of transport assays that test the predictions (Fig. 4). In wild type (WT), BBS proteins maintain IFT particle integrity by antagonizing the mechanical competition between kinesin-II and OSM-3. In *bbs-7/-8* single mutants, mechanical competition between kinesin-II and OSM-3 is not counterbalanced by BBS proteins, so IFT particles dissociate into subcomplexes A and B. In *bbs-7/-8;kinesin-II* or *bbs-7/-8;osm-3* double mutants, no mechanical competition is generated, so IFT particles do not dissociate but are moved by kinesin-II or OSM-3 alone.

A Predictions

	Alternating Action	Mechanical Competition
bbs-; klp-11	**B** OSM-3-kinesin 1. IFT-A does not move; 2. Ciliary lengths decrease; 3. More severe aggregation. Axonemal Microtubules	**A B** OSM-3-kinesin Both IFT-A and IFT-B move at the fast rate of OSM-3. Axonemal Microtubules
bbs-; osm-3	**A** Kinesin-II 1. IFT-B does not move; 2. Ciliary lengths decrease. Axonemal Microtubules	**A B** Kinesin-II Both IFT-A and IFT-B move at the slow rate of Kinesin-II. Axonemal Microtubules

B Results

WT

$F_{holding (BBS)} = F_{separating (Motors)}$

BBS — **A B** — Kinesin-II — OSM-3-kinesin — Axonemal Microtubules

bbs

$F_{holding (BBS)} = 0 < F_{separating (Motors)}$

A B — Kinesin-II — OSM-3-kinesin — Axonemal Microtubules

bbs;klp-11

A B — No holding or separating forces — OSM-3-kinesin — Axonemal Microtubules

bbs;osm-3

A B — Kinesin-II — No holding or separating forces — Axonemal Microtubules

to the *klp-11* and *osm-3* mutants, respectively. In particular, the *bbs-7/-8;klp-11* double mutants have almost full-length cilia, which is similar to the *klp-11* mutants, and the *bbs-7/-8;osm-3* double mutants have truncated cilia similar to the *osm-3* mutants. (2) Unlike in the *bbs-7/-8* single mutants, in the *bbs-7/-8;klp-11* and *bbs-7/-8;osm-3* double mutants, the IFT particles remain intact, and the IFT-A and -B subcomplexes move together at an identical rate, which is characteristic of OSM-3 or kinesin-II, respectively (Fig. 4 and Table III).

These results support the predictions of the mechanical competition model (Fig. 3 B). Accordingly, we propose that in wild-type *C. elegans*, IFT particles are moved along sensory cilia by kinesin-II and OSM-3–kinesin acting together, with the slower moving kinesin-II exerting drag on the faster moving OSM-3, whereas the faster moving OSM-3 tends to pull the slower moving kinesin-II along (Fig. 3 B). This produces a mechanical competition that translates into tension across the IFT particles, leading to their dissociation in the absence of the BBS proteins (Fig. 3 B, *bbs* mutant). Thus, the BBS-7 and -8 proteins antagonize this tension force and maintain the integrity of the IFT particles by stabilizing the association of IFT-A with IFT-B (Fig. 3 B, wild type [WT]). Conversely, in

bbs-7 or *-8* single mutants, this stabilization is lost, and the motor-dependent stresses dissociate subcomplexes A and B, which are moved separately by kinesin-II or OSM-3 (Fig. 3 B). In the *bbs;kinesin-2* double mutants, however, the remaining kinesin-2 motor lacks its antagonistic partner, so the stresses required to dissociate IFT-A from IFT-B are absent. Consequently, the IFT particles are moved intact along the cilium by kinesin-II or OSM-3–kinesin alone (Fig. 3 B, *bbs;klp-11* and *bbs;osm-3*).

Discussion

Kinesin-II and OSM-3 cooperate to drive intermediate rates of motility in vivo and in vitro

This study used competitive motility assays, quantitative modeling, and in vivo transport assays in ciliary mutants to investigate how kinesin-II and OSM-3 cooperate to move IFT particles along the initial segment of the cilium. This required purified kinesin-II (this study) and OSM-3 kinesin (Imanishi et al., 2006). Native kinesin-II had been purified from sea urchin embryos (Cole et al., 1992, 1993; Rashid et al., 1995; Wedaman et al., 1996)
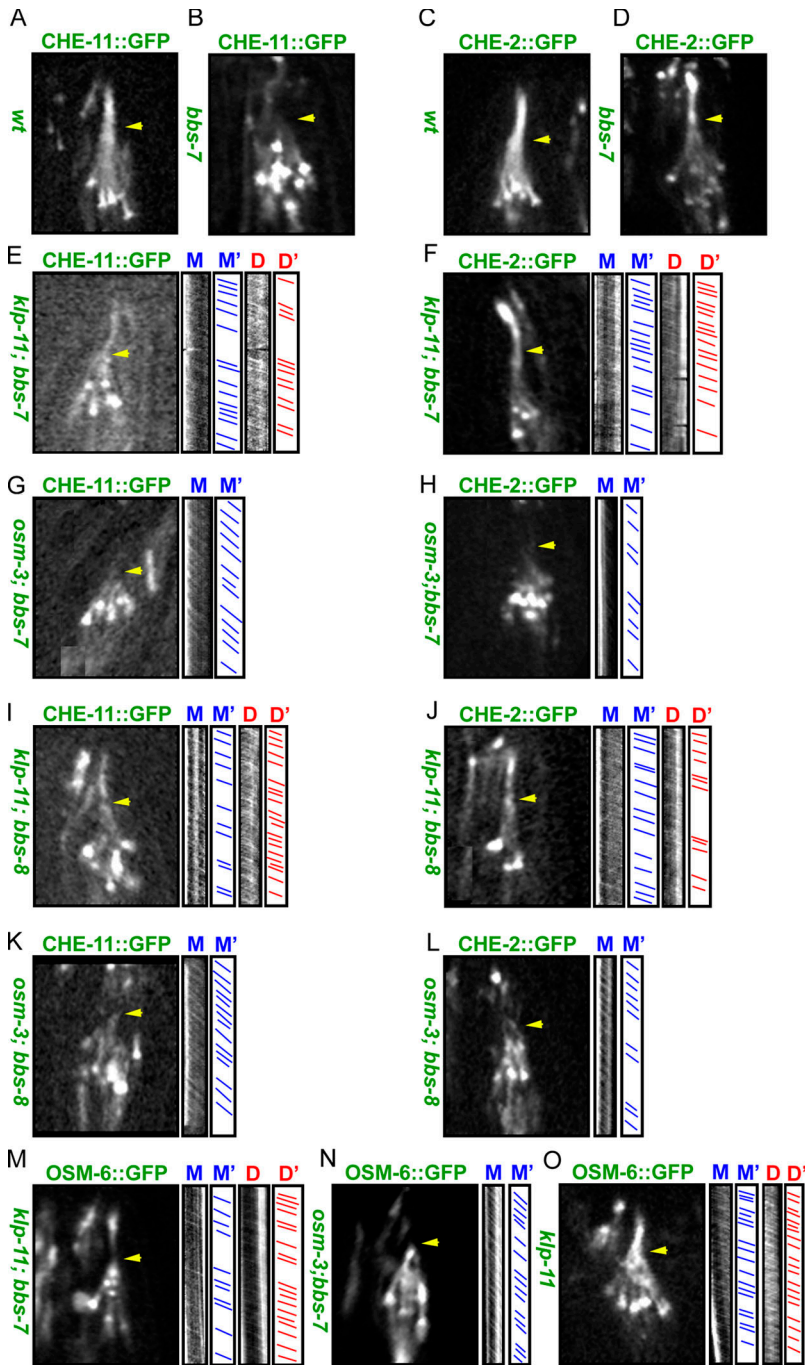
Figure 4. **Transport assays of IFT particle subcomplexes A and B in *bbs-7* single and *bbs-7* or *bbs-8*; *kinesin-2* double mutants.** Micrographs of the distribution of IFT-A (CHE-11::GFP) and -B (CHE-2::GFP and OSM-6::GFP) subcomplexes along sensory cilia (CHE-11::GFP in A, B, E, G, I, and K; CHE-2::GFP in C, D, F, H, J, and L; and OSM-6::GFP in M–O). Kymographs and corresponding graphs in E–O (right) show the diagonal lines that represent trajectories of movement along the initial (M and M') and distal segments (D and D'). Arrowheads point to initial-distal segment junctions. In wild-type (wt) animals (A and C), CHE-11::GFP and CHE-2::GFP move identically along initial and distal segments. In *bbs-7* mutants (B and D), IFT-A and -B dissociate, CHE-11::GFP only moves within the initial segment, and CHE-2::GFP moves along both the initial and distal segments. In *klp-11;bbs-7* or *bbs-8* double mutants, CHE-11::GFP, CHE-2::GFP, and OSM-6::GFP move at OSM-3–kinesin's fast velocity along the initial and distal segment (E, F, I, J, and M). In *osm-3; bbs-7* or *bbs-8* double mutants, CHE-11::GFP, CHE-2::GFP, and OSM-6::GFP move at kinesin-II's slow rate in the remaining initial segment (G, H, K, L, and N). OSM-6::GFP moves at OSM-3's fast rate in *klp-11* mutants (O). Unlike in *bbs* single mutants, IFT particles are stable and do not dissociate into IFT-A and -B in *bbs-7* or *bbs-8*; *kinesin-2* double mutants.

and subsequently from other systems (Kondo et al., 1994; Yamazaki et al., 1996; Cole et al., 1998; Pierce et al., 1999; Signor et al., 1999; Berezuk and Schroer, 2004; Zhang and Hancock, 2004) in amounts that allowed the basic motility properties of several members of the kinesin-2 family to be analyzed, but the low abundance of native *C. elegans* kinesin-II precluded motility assays (Signor et al., 1999). This problem was circumvented here using baculovirus expression.

The availability of purified *C. elegans* kinesin-II and OSM-3 allowed us to assess their role in IFT by comparing in vivo and in vitro motility assays. The rates of MT gliding driven by kinesin-II and OSM-3 (0.4–0.5 and 1.1 μm/s) are similar

to the rates of anterograde movement of GFP::kinesin-II and GFP::OSM-3 alone along *C. elegans* sensory cilia (0.5 and 1.3 μm/s), and the intermediate rate of 0.7 μm/s seen along the initial segment of the cilium can be recapitulated in gliding assays using mixtures of kinesin-II and OSM-3 (Orozco et al., 1999; Snow et al., 2004; Ou et al., 2005). This is striking given the different conditions under which the motors drive MT gliding over glass coverslips versus driving IFT particle transport along cilia, where different ATP concentrations, different MT tracks, and the presence of IFT particles or other regulatory cofactors could influence motility. Both quantitative modeling and in vivo IFT assays using *bbs;IFT motor* double mutants are

Table III. **Velocity of IFT particle proteins in *bbs* and *kinesin-2* mutant animals**

Anterograde motility	Strain	Mean velocities			
		Initial segment	*n*	Distal segment	*n*
		$\mu m/s^{-1}$		$\mu m/s^{-1}$	
IFT-A					
CHE-11::GFP	Wild type[a]	~0.70		~1.30	
	bbs-7 or *bbs-8*[a]	~0.50–0.60		None	
	bbs-7;osm-3	0.56 ± 0.06	103	None	
	bbs-8;osm-3	0.52 ± 0.05	110	None	
	bbs-7;klp-11	1.27 ± 0.16	103	1.34 ± 0.17	107
	bbs-8;klp-11	1.26 ± 0.19	101	1.34 ± 0.19	104
IFT-B					
CHE-2::GFP	Wild type[a]	~0.70		~1.30	
	bbs-7 or *bbs-8*[a]	~1.10–1.30		~1.30	
	bbs-7;klp-11	1.30 ± 0.18	107	1.35 ± 0.18	102
	bbs-8;klp-11	1.22 ± 0.17	110	1.28 ± 0.16	104
	bbs-7;osm-3	0.51 ± 0.07	105	None	
	bbs-8;osm-3	0.55 ± 0.06	102	None	
OSM-6::GFP	Wild type[b]	~0.70		~1.30	
	osm-3[b]	~0.50		None	
	klp-11	1.28 ± 0.15	107	1.33 ± 0.15	106
	bbs-7	1.18 ± 0.17	104	1.32 ± 0.19	101
	bbs-7;osm-3	0.55 ± 0.07	109	None	
	bbs-7;klp-11	1.28 ± 0.16	100	1.22 ± 0.17	101

[a]Ou et al., 2005.
[b]Snow et al., 2004.

concordant with the intermediate rate being caused by simple mechanical competition between kinesin-II and OSM-3, which further suggests that motor coordination does not require sophisticated regulatory mechanisms to turn the motors on and off.

Role of BBS proteins in IFT particle stability and motor coordination

In this model, BBS proteins coordinate the motors simply by maintaining the association of kinesin-II–IFT-A with OSM-3–IFT-B, which otherwise dissociate because of tension exerted by the two motors (e.g., in *bbs* mutants). In gliding assays, BBS proteins are not required because the coverslip forms a physical connection between adjacent kinesin-II and OSM-3 proteins. Our model assumes that IFT subcomplexes A and B normally interact to form a single IFT particle complex that is moved along the wild-type cilium by both kinesin-II and OSM-3 (which may move along the MT A and B subfibers, respectively; Ou et al., 2005). However, although IFT particles isolated from *Chlamydomonas reinhardtii* flagella (which probably lack BBS proteins) sediment as a 16-S complex, they can also be separated by varying the solution conditions, raising the possibility that IFT-A and -B usually exist as separate complexes in vivo (Cole et al., 1998; Qin et al., 2004). For example, our previous data could be explained if in wild types, separate complexes of kinesin-II–OSM-3–IFT-A and kinesin-II–OSM-3–IFT-B move at the same rate along the initial segment of the cilium, with BBS proteins being required to dock OSM-3 onto the kinesin-II–IFT-B complex and kinesin-II onto the OSM-3–kinesin-II complex (Ou et al., 2005). However, this predicts that in *bbs;kinesin-II* and *bbs;osm-3* double

mutants, IFT-A and -B, respectively, would not move along the cilium at all, which is inconsistent with our IFT assays. More work is required to firmly establish that IFT-A and -B normally interact to form a single transport complex in vivo.

Although BBS proteins appear to be required for the stabilization of IFT particles in systems that use both kinesin-II and OSM-3 for ciliogenesis, in organisms where kinesin-II acts alone (for example, *C. reinhardtii*), the two-motor–dependent mechanical competition is lacking, so IFT particles should remain intact in *bbs* mutants, and BBS proteins may not be needed. Indeed, BBS-7/-8 proteins are absent in the *C. reinhardtii* flagellome (Pazour et al., 2005), although it is possible that they, along with OSM-3, enter the flagellum and elongate distal singlets during mating (Mesland et al., 1980). In vertebrates, the OSM-3 homologue KIF17 is required to target cyclic nucleotide-gated channels to the cilium (Jenkins et al., 2006). Moreover, prominent distal singlets of the type found in *C. elegans* sensory cilia occur in various organisms (e.g., human [Moran et al., 1982] and frog olfactory cilia [Reese, 1965]), and cyclic nucleotide-gated channels cluster over a region of the distal segments in the latter cilia (Flannery et al., 2006). Interestingly, BBS knockout mice (BBS-1, -2, and -4) specifically lose the distal segments of their olfactory cilia, which results in anosmia (Kulaga et al., 2004; Mykytyn et al., 2004; Nishimura et al., 2004). Thus, BBS proteins may contribute to IFT specifically in cilia containing distal segments, where two anterograde IFT motors are used. The BBS protein–dependent mechanical competition between IFT motors, which was uncovered in *C. elegans* sensory neurons, may be relevant to the assembly of

similar two-domain cilia in some vertebrates in which defects in this process may underlie BBS.

Relevance to other systems of motor coordination

The antagonistic competition between opposite polarity mitotic MT motors has been discussed extensively (Sharp et al., 2000), and precedents also exist for functional interaction between same-polarity motors. In muscles, for example, slower cycling cross-bridges can exert drag on faster cycling bridges and, thereby, slow down the maximal velocity of the shortening of the muscle (Warshaw et al., 1990). It has also been shown that a motor can be accelerated by a force applied in the direction of MT gliding driven by that motor (Coppin et al., 1997). Moreover, the biophysical plausibility of our proposed mechanism is supported by experiments in which plus end–directed kinesin motors with different speeds were shown to interact to produce intermediate speeds in motility assays, including kinesin-1 and -5 (Crevel et al., 2004) and mixed Kif3A and Kif3B homodimers (Zhang and Hancock, 2004). The striking studies of Zhang and Hancock (2004) illuminate how the distinct Kif3A and Kif3B motor domains can cooperate within the processive kinesin-II holoenzyme, but the competition between kinesin-1 versus kinesin-5 and Kif3A versus Kif3B homodimers are unlikely to reflect true in vivo interactions. To our knowledge, our study is the first to uncover competitive motility between distinct, same-polarity MT-based intracellular transport motor holoenzymes that are known to cooperate in vivo.

This system differs from the controlled coordination that exists between kinesin-II and cytoplasmic dynein on melanosomes (Rogers et al., 1997) and other cargoes (Kural et al., 2005), in which the simultaneous activation and inhibition of the anterograde and retrograde motors (and vice versa) facilitates alternating runs in the anterograde and retrograde direction (Mallik and Gross, 2004). The distinct mechanical competition proposed here for same-polarity IFT motors may represent yet another general way in which motors are coordinated and controlled to produce coherent networks of intracellular transport within eukaryotic cells.

Model predictions

The quantitative mechanical competition model makes testable predictions. For example, the unloaded velocities of kinesin-II and OSM-3, $V_{kinesin-II}^{max}$ and V_{OSM-3}^{max}, are known, but the ratio of their stall forces, γ, is an unknown free parameter (supplemental material). By adjusting γ and comparing the resulting curve to the gliding assay data, we find the best fit when the ratio of OSM-3 to kinesin-II stall forces is

$$\gamma = \frac{F_{osm-3}^{max}}{F_{kinesin-II}^{max}} = 0.98 \approx 1$$

suggesting that kinesin-II and OSM-3 stall at similar forces, which can be tested in future experiments. We can also estimate the molar ratio of OSM-3 and kinesin-II on IFT particles by combining (1) the stall force ratio ($\gamma = 0.98$), (2) the unloaded

velocities of the two motors ($V_{osm-3}^{max} = 1.3$ μm/s and $V_{kinesin-II}^{max} = 0.5$ μm/s), and (3) the velocity of IFT particle transport driven by the concerted action of the two motors ($v_{cargo} = 0.72$ μm/s, yielding C = 1.25). This leads to the prediction that in vivo, the mole fraction of OSM-3 is $\alpha \approx 0.45$, reflecting an approximately equimolar ratio of the two motors on the IFT particles within the initial segment of the cilium. The analysis of isolated motor–IFT particle complexes may allow us to test this prediction.

Overall, this work illuminates how two anterograde IFT motors cooperate to move IFT particles along the initial segment of the axoneme at a rate that is intermediate between the free-sliding rate of each motor alone to build the cilium foundation on dendritic endings of *C. elegans* sensory neurons.

Materials and methods

Purification of recombinant kinesin-II from Sf9 cells

Sf9 cells infected with baculovirus containing the three genes *klp-11*, *klp-20*, and *kap-1* that encode kinesin-II expressed sufficient quantities of the corresponding subunits to permit the purification of the heterotrimeric complex in a monodisperse, active state in high yields (Fig. 1). To accomplish this, PCR amplifications containing the cDNA sequences for KAP-1, KLP-11, and KLP-20 (GenBank/EMBL/DDBJ accession no. NM_001026075, NM_171407, and NM_064777, respectively) were inserted into Gateway vector pDONR221 (Invitrogen) and cloned into target vector pDEST8 (Invitrogen), and recombinant baculoviruses were generated according to the manufacturer's instructions. The infected cells were then incubated for 3 d at 27°C before being harvested.

Cell pellets from 400 ml of culture were suspended in 80 ml of ice-cold lysis buffer containing 50 mM Pipes, pH 7.0, 300 mM NaCl, 1 mM MgCl₂, 1 mM 2-mercaptoethanol, and EDTA-free protease inhibitor mixture (Roche) and passed twice through a French press at 1,000 pounds per square inch. The cell lysate was centrifuged for 30 min at 1,5000 *g* and 4°C. The supernatant was purified using Talon affinity beads (BD Biosciences) according to the manufacturer's instructions. The Talon-purified protein was dialyzed against gel filtration column buffer containing 80 mM Pipes, pH 6.9, 200 mM NaCl, 1 mM MgCl₂, 1 mM EGTA, 1 mM DTT, and 0.1 mM ATP. The kinesin-II complex was further purified on a column (Sephacryl S-300HR; GE Healthcare) in gel filtration buffer and concentrated by ultrafiltration with Centriprep 30K (Amicon). This simple procedure of Talon column affinity followed by Sephacryl S-300 gel filtration chromatography routinely yielded 2 mg of highly purified kinesin-II per 400 ml of starting material (Fig. 1 A and Fig. S1 A). We estimate that we would need to start with 4,000 liters of mixed stage worm culture (i.e., 10,000 times more starting material) to purify kinesin-II in comparable amounts (Signor et al., 1999).

Hydrodynamic analysis

Sucrose density gradient centrifugation and gel filtration chromatography were performed as described previously (Wedaman et al., 1996). The molecular weight of the kinesin-II complex was calculated using the Siegel and Monty equation (Siegel and Monty, 1966; Cole et al., 1992; Wedaman et al., 1996).

Motility assays

MT motility assays were performed as described previously at 21°C (Cohn et al., 1989). The velocities of 10–60 MTs were measured for each data point.

Fluorescence microscopy

IFT was assayed as described previously (Snow et al., 2004; Ou et al., 2005). The GFP transgenic worms were anesthetized with 10 mM levamisole, mounted on agar pads, and maintained at 21°C. We collected images with a microscope (IX70; Olympus) equipped with a 100× NA 1.35 objective and a spinning disc confocal head (UltraVIEW; PerkinElmer) with excitation by 488-argon ion lasers at 0.3 s/frame for 2–3 min. All images were acquired using cooled charge-coupled device cameras (ORCA-ER; Hamamatsu), and kymographs and videos were created using MetaMorph software (Universal Imaging Corp.).

Creation and maintenance of *bbs* and motor mutant animals

Transgenic animals expressing *che-11::gfp, che-2::gfp*, and *osm-6::gfp* were crossed with *bbs-7/osm-12(n1606), bbs-8(nx77)* and *klp-11(tm324),* or *osm-3(p802)* to create double mutants, and their genotypes were confirmed by their dye-filling phenotype and/or PCR.

Online supplemental material

Supplemental material provides data (1) supporting purified *C. elegans* kinesin-II as a monodisperse heterotrimeric complex whose motility conforms to Michaelis-Menten kinetics and (2) describing quantitative models for the functional coordination of the two anterograde IFT kinesins. Fig. S1 shows the purification and hydrodynamic analysis of the heterotrimeric kinesin-II from Sf9 cell extracts. Fig. S2 shows Michaelis-Menten analysis of the motility activity of purified *C. elegans* kinesin-II in the presence and absence of nucleotide substrates and inhibitors. Fig. S3 shows the alternating action and mechanical competition models that explain the comovement of kinesin-II and OSM-3–kinesin along sensory cilia. Fig. S4 shows motility assay data obtained using kinesin-II or OSM-3 alone and mixtures of the two motors together with the gliding velocity versus mole fraction relationship. Video 1 shows in vitro assays of MT gliding induced by purified kinesin-II, purified OSM-3, and a mixture of the two motors. Videos 2–5 show in vivo transport assays of the movement of IFT particle proteins along sensory cilia of double mutant strains *bbs-7(n1606);klp-11(tm324)* and *bbs-7(n1606);osm-3(p802).* Online supplemental material is available at http://www.jcb.org/cgi/content/full/jcb.200606003/DC1.

References

Ansley, S.J., J.L. Badano, O.E. Blacque, J. Hill, B.E. Hoskins, C.C. Leitch, J.C. Kim, A.J. Ross, E.R. Eichers, T.M. Teslovich, et al. 2003. Basal body dysfunction is a likely cause of pleiotropic Bardet-Biedl syndrome. *Nature*. 425:628–633.

Badano, J.L., N. Mitsuma, P.L. Beales, and N. Katsanis. 2006. The ciliopathies: an emerging class of human genetic disorders. *Annu. Rev. Genomics. Hum. Genet.* 7:125–148.

Beales, P.L. 2005. Lifting the lid on Pandora's box: the Bardet-Biedl syndrome. *Curr. Opin. Genet. Dev.* 15:315–323.

Berezuk, M.A., and T.A. Schroer. 2004. Fractionation and characterization of kinesin II species in vertebrate brain. *Traffic.* 5:503–513.

Blacque, O.E., M.J. Reardon, C. Li, J. McCarthy, M.R. Mahjoub, S.J. Ansley, J.L. Badano, A.K. Mah, P.L. Beales, W.S. Davidson, et al. 2004. Loss of *C. elegans* BBS-7 and BBS-8 protein function results in cilia defects and compromised intraflagellar transport. *Genes Dev.* 18:1630–1642.

Bray, D., and T. Duke. 2004. Conformational spread: the propagation of allosteric states in large multiprotein complexes. *Annu. Rev. Biophys. Biomol. Struct.* 33:53–73.

Cohn, S.A., A.L. Ingold, and J.M. Scholey. 1989. Quantitative analysis of sea urchin egg kinesin-driven microtubule motility. *J. Biol. Chem.* 264:4290–4297.

Cole, D.G., W.Z. Cande, R.J. Baskin, D.A. Skoufias, C.J. Hogan, and J.M. Scholey. 1992. Isolation of a sea urchin egg kinesin-related protein using peptide antibodies. *J. Cell Sci.* 101:291–301.

Cole, D.G., S.W. Chinn, K.P. Wedaman, K. Hall, T. Vuong, and J.M. Scholey. 1993. Novel heterotrimeric kinesin-related protein purified from sea urchin eggs. *Nature*. 366:268–270.

Cole, D.G., D.R. Diener, A.L. Himelblau, P.L. Beech, J.C. Fuster, and J.L. Rosenbaum. 1998. *Chlamydomonas* kinesin-II-dependent intraflagellar transport (IFT): IFT particles contain proteins required for ciliary assembly in *Caenorhabditis elegans* sensory neurons. *J. Cell Biol.* 141:993–1008.

Coppin, C.M., D.W. Pierce, L. Hsu, and R.D. Vale. 1997. The load dependence of kinesin's mechanical cycle. *Proc. Natl. Acad. Sci. USA*. 94:8539–8544.

Crevel, I.M., M.C. Alonso, and R.A. Cross. 2004. Monastrol stabilises an attached low-friction mode of Eg5. *Curr. Biol.* 14:R411–R412.

Evans, J.E., J.J. Snow, A.L. Gunnarson, G. Ou, H. Stahlberg, K.L. McDonald, and J.M. Scholey. 2006. Functional modulation of IFT kinesins extends the sensory repertoire of ciliated neurons in *Caenorhabditis elegans*. *J. Cell Biol.* 172:663–669.

Flannery, R.J., D.A. French, and S.J. Kleene. 2006. Clustering of cyclic-nucleotide-gated channels in olfactory cilia. *Biophys. J.* 91:179–188.

Howard, J. 2001. Mechanics of Motor Proteins and the Cytoskeleton. Sinauer Associates, Sunderland, MA. 367 pp.

Imanishi, M., N. Endres, A. Gennerich, and R. Vale. 2006. Autoinhibition regulates the motility of the *C. elegans* intraflagellar transport motor OSM-3. *J. Cell Biol.* 174:931–937.

Jenkins, P.M., T.W. Hurd, L. Zhang, D.P. McEwen, R.L. Brown, B. Margolis, K.J. Verhey, and J.R. Martens. 2006. Ciliary targeting of olfactory CNG channels requires the CNGB1b subunit and the kinesin-2 motor protein, KIF17. *Curr. Biol.* 16:1211–1216.

Kondo, S., R. Sato-Yoshikate, Y. Noda, H. Aizawa, T. Nakata, Y. Matsuura, and N. Hirokawa. 1994. KIF3A is a new microtubule-based anterograde motor in the nerve axon. *J. Cell Biol.* 125:1095–1107.

Kulaga, H.M., C.C. Leitch, E.R. Eichers, J.L. Badano, A. Lesemann, B.E. Hoskins, J.R. Lupski, P.L. Beales, R.R. Reed, and N. Katsanis. 2004. Loss of BBS proteins causes anosmia in humans and defects in olfactory cilia structure and function in the mouse. *Nat. Genet.* 36:994–998.

Kural, C., H. Kim, S. Syed, G. Goshima, V.I. Gelfand, and P.R. Selvin. 2005. Kinesin and dynein move a peroxisome in vivo: a tug-of-war or coordinated movement? *Science*. 308:1469–1472.

Lawrence, C.J., R.K. Dawe, K.R. Christie, D.W. Cleveland, S.C. Dawson, S.A. Endow, L.S. Goldstein, H.V. Goodson, N. Hirokawa, J. Howard, et al. 2004. A standardized kinesin nomenclature. *J. Cell Biol.* 167:19–22.

Mallik, R., and S.P. Gross. 2004. Molecular motors: strategies to get along. *Curr. Biol.* 14:R971–R982.

Mallik, R., B.C. Carter, S.A. Lex, S.J. King, and S.P. Gross. 2004. Cytoplasmic dynein functions as a gear in response to load. *Nature*. 427:649–652.

Mesland, D.A., J.L. Hoffman, E. Caligor, and U.W. Goodenough. 1980. Flagellar tip activation stimulated by membrane adhesions in *Chlamydomonas* gametes. *J. Cell Biol.* 84:599–617.

Moran, D.T., J.C. Rowley III, B.W. Jafek, and M.A. Lovell. 1982. The fine structure of the olfactory mucosa in man. *J. Neurocytol.* 11:721–746.

Mykytyn, K., R.F. Mullins, M. Andrews, A.P. Chiang, R.E. Swiderski, B. Yang, T. Braun, T. Casavant, E.M. Stone, and V.C. Sheffield. 2004. Bardet-Biedl syndrome type 4 (BBS4)-null mice implicate Bbs4 in flagella formation but not global cilia assembly. *Proc. Natl. Acad. Sci. USA*. 101:8664–8669.

Nishimura, D.Y., M. Fath, R.F. Mullins, C. Searby, M. Andrews, R. Davis, J.L. Andorf, K. Mykytyn, R.E. Swiderski, B. Yang, et al. 2004. Bbs2-null mice have neurosensory deficits, a defect in social dominance, and retinopathy associated with mislocalization of rhodopsin. *Proc. Natl. Acad. Sci. USA*. 101:16588–16593.

Orozco, J.T., K.P. Wedaman, D. Signor, H. Brown, L. Rose, and J.M. Scholey. 1999. Movement of motor and cargo along cilia. *Nature*. 398:674.

Ou, G., O.E. Blacque, J.J. Snow, M.R. Leroux, and J.M. Scholey. 2005. Functional coordination of intraflagellar transport motors. *Nature*. 436:583–587.

Pan, J., Q. Wang, and W.J. Snell. 2005. Cilium-generated signaling and cilia-related disorders. *Lab. Invest.* 85:452–463.

Pazour, G.J., N. Agrin, J. Leszyk, and G.B. Witman. 2005. Proteomic analysis of a eukaryotic cilium. *J. Cell Biol.* 170:103–113.

Perkins, L.A., E.M. Hedgecock, J.N. Thomson, and J.G. Culotti. 1986. Mutant sensory cilia in the nematode *Caenorhabditis elegans*. *Dev. Biol.* 117:456–487.

Pierce, D.W., N. Hom-Booher, A.J. Otsuka, and R.D. Vale. 1999. Single-molecule behavior of monomeric and heteromeric kinesins. *Biochemistry*. 38:5412–5421.

Qin, H., D.R. Diener, S. Geimer, D.G. Cole, and J.L. Rosenbaum. 2004. Intraflagellar transport (IFT) cargo: IFT transports flagellar precursors to the tip and turnover products to the cell body. *J. Cell Biol.* 164:255–266.

Rashid, D.J., K.P. Wedaman, and J.M. Scholey. 1995. Heterodimerization of the two motor subunits of the heterotrimeric kinesin, KRP85/95. *J. Mol. Biol.* 252:157–162.

Reese, T.S. 1965. Olfactory cilia in the frog. *J. Cell Biol.* 25:209–230.

Rogers, S.L., I.S. Tint, P.C. Fanapour, and V.I. Gelfand. 1997. Regulated bidirectional motility of melanophore pigment granules along microtubules in vitro. *Proc. Natl. Acad. Sci. USA*. 94:3720–3725.

Rosenbaum, J.L., and G.B. Witman. 2002. Intraflagellar transport. *Nat. Rev. Mol. Cell Biol.* 3:813–825.

Scholey, J.M. 2003. Intraflagellar transport. *Annu. Rev. Cell Dev. Biol.* 19:423–443.

Scholey, J.M., and K.V. Anderson. 2006. Intraflagellar transport and cilium-based signaling. *Cell*. 125:439–442.

Shakir, M.A., T. Fukushige, H. Yasuda, J. Miwa, and S.S. Siddiqui. 1993. *C. elegans* osm-3 gene mediating osmotic avoidance behaviour encodes a kinesin-like protein. *Neuroreport*. 4:891–894.

Sharp, D.J., G.C. Rogers, and J.M. Scholey. 2000. Microtubule motors in mitosis. *Nature*. 407:41–47.

Siegel, L.M., and K.J. Monty. 1966. Determination of molecular weights and frictional ratios of proteins in impure systems by use of gel filtration and density gradient centrifugation. Application to crude preparations of sulfite and hydroxylamine reductases. *Biochim. Biophys. Acta*. 112:346–362.

Signor, D., K.P. Wedaman, L.S. Rose, and J.M. Scholey. 1999. Two heteromeric kinesin complexes in chemosensory neurons and sensory cilia of *Caenorhabditis elegans*. *Mol. Biol. Cell*. 10:345–360.

Singh, M.P., R. Mallik, S.P. Gross, and C.C. Yu. 2005. Monte Carlo modeling of single-molecule cytoplasmic dynein. *Proc. Natl. Acad. Sci. USA*. 102:12059–12064.

Snow, J.J., G. Ou, A.L. Gunnarson, M.R. Walker, H.M. Zhou, I. Brust-Mascher, and J.M. Scholey. 2004. Two anterograde intraflagellar transport motors cooperate to build sensory cilia on *C. elegans* neurons. *Nat. Cell Biol.* 6:1109–1113.

Svoboda, K., and S.M. Block. 1994. Force and velocity measured for single kinesin molecules. *Cell*. 77:773–784.

Vale, R.D., T.S. Reese, and M.P. Sheetz. 1985. Identification of a novel force-generating protein, kinesin, involved in microtubule-based motility. *Cell*. 42:39–50.

Valentine, M.T., P.M. Fordyce, T.C. Krzysiak, S.P. Gilbert, and S.M. Block. 2006. Individual dimers of the mitotic kinesin motor Eg5 step processively and support substantial loads in vitro. *Nat. Cell Biol.* 8:470–476.

Warshaw, D.M., J.M. Desrosiers, S.S. Work, and K.M. Trybus. 1990. Smooth muscle myosin cross-bridge interactions modulate actin filament sliding velocity in vitro. *J. Cell Biol.* 111:453–463.

Wedaman, K.P., D.W. Meyer, D.J. Rashid, D.G. Cole, and J.M. Scholey. 1996. Sequence and submolecular localization of the 115-kD accessory subunit of the heterotrimeric kinesin-II (KRP85/95) complex. *J. Cell Biol.* 132:371–380.

Yamazaki, H., T. Nakata, Y. Okada, and N. Hirokawa. 1996. Cloning and characterization of KAP3: a novel kinesin superfamily-associated protein of KIF3A/3B. *Proc. Natl. Acad. Sci. USA*. 93:8443–8448.

Zhang, Y., and W.O. Hancock. 2004. The two motor domains of KIF3A/B coordinate for processive motility and move at different speeds. *Biophys. J.* 87:1795–1804.